Electrochimica Acta 262 (2018) 173–181

Contents lists available at ScienceDirect

Electrochimica Acta

journal homepage: www.elsevier.com/locate/electacta

Nanosized graphene sheets induced high electrochemical activity in pure carbon film

Liangliang Huang [a, b], Yuanyuan Cao [a], Dongfeng Diao [a, *]

[a] Institute of Nanosurface Science and Engineering (INSE), Shenzhen University, Shenzhen 518060, China
[b] Key Laboratory of Optoelectronic Devices and Systems of Ministry of Education and Guangdong Province, College of Optoelectronic Engineering, Shenzhen University, Shenzhen 518060, China

ARTICLE INFO

Article history:
Received 22 October 2017
Received in revised form
2 January 2018
Accepted 4 January 2018
Available online 5 January 2018

Keywords:
Graphene
Carbon film
Electrochemical activity
Biosensor

ABSTRACT

We found that nanosized graphene sheets induced high electrochemical activity in pure carbon films, which prepared by electron cyclotron resonance (ECR) plasma sputtering under low-energy electron irradiation condition. The electrochemical properties were studied by electrochemical impedance spectroscopy and cyclic voltammetry. The graphene sheets embedded carbon (GSEC) films showed a wide potential window over 3.2 V. The charge transfer resistance and the oxidation-reduction peak separation (ΔE_P) of the GSEC films are lower than amorphous carbon films in several redox systems ($Fe(CN)_6^{4-/3-}$, $Ru(NH_3)_6^{2+/3+}$, dopamine and ascorbic acid), especially in the inner-sphere system, the ΔE_P is only half of amorphous carbon films. The high electrochemical activity of GSEC films originated from the nanosized graphene sheets, which offered faster electron transfer path and more reaction active sites. Our results indicate the GSEC films have great potential to be an electrochemical biosensor in detecting biomolecules with high oxidation potential.

1. Introduction

Carbon films have been widely investigated due to their excellent performance in electrochemical measurements, such as wide potential window, low background current and high reproducibility [1]. However, limited by the electrochemical activity, carbon films can't be widely applied [2]. In the last decade, some new depositing methods have been developed to optimize the film structures for improving the electrochemical activity. A carbon film with nanocrystalline structures prepared by electron cyclotron resonance (ECR) plasma sputtering with ion irradiation [3,4] was proposed. Comparing with the classical glassy carbon (GC), the special sp^2 and sp^3 mixed bonds structure make this film better in electrochemical activity with a lower background current, a wider potential window (4.1 V). The similar films have also been prepared with unbalanced magnetron sputtering by Niwa O et al. [5,6]. The nanocrystlline is the key which improved the electrochemical activity of carbon films. Furthermore, the graphene has better electrochemical activity than other carbon materials [7,8]. Hence, many efforts have been devoted to improving the electrochemical activity of carbon materials by doping graphene. Yildiz et al. [9] modified the carbon paste electrodes with graphene, and successfully applied them in pharmaceutical analysis. Sheng Z [10] and other researchers [11,12] found graphene, nitrogen doped graphene and reduced graphene oxide all can effective improve the electrochemical activity of GC. However, there are few methods to form graphene structure in-situ in carbon films so far. In-situ forming graphene in carbon film, not only can improve the electrochemical activity significantly, but also is helpful to maintain the inherent properties of carbon film. Recently, we have developed a method for in-situ depositing graphene sheets embedded carbon (GSEC) film, which is low energy electron irradiation ECR plasma sputtering (EI-ECR) [13,14]. Unlike the ion irradiation, the energy of electron irradiation is low, which beneficial to form graphene sheets [13]. Furthermore, the size of graphene sheets can be simply controlled by adjusting the energy of electron irradiation [13,15]. The graphene sheets induced the pure carbon film possessed special tribological performance [16], photoelectric [14] and electromagnetic properties [17]. However, up to now, there was no report focus on the effects of nanosized graphene sheets on the electrochemical properties of carbon films.

In this paper, we investigated the electrochemical properties of nanosized GSEC films by comparing with ion irradiation ECR (II-

* Corresponding author.
E-mail address: dfdiao@szu.edu.cn (D. Diao).

https://doi.org/10.1016/j.electacta.2018.01.027
0013-4686/

ECR) carbon films. The structure was characterized by atomic force microscopy (AFM), transmission electron microscopy (TEM), Raman spectra and X-ray photoelectron spectroscopy (XPS). The electrochemical impedance spectroscopy (EIS) was measured in 5 mM $Fe(CN)_6^{4-/3-}$. The potential windows were tested in 0.05 M H_2SO_4 solutions. The electrochemical activity was studied by cyclic voltammetry with several redox probes encompassing both outer-sphere ($Ru(NH_3)_6^{2+/3+}$) and inner-sphere ($Fe(CN)_6^{4-/3-}$, dopamine (DA) and ascorbic acid (AA)) redox systems. At last, we applied this carbon film in measuring 5-Methylcytosine, which was difficult to measure electrochemically because of their high oxidation potential.

2. Experimental

2.1. Carbon film preparation

The carbon films were deposited on Si (100) with ECR plasma sputtering technique. Prior to the deposition, the chamber was pumped to a background pressure of 8.0×10^{-5} Pa and purity argon was introduced into the chamber as the working gas with a pressure of 4.00×10^{-2} Pa. During the deposition, a DC bias voltage of −500 V was applied to the carbon target. The EI-ECR carbon films were fabricated at bias voltage of +50 V and +20 V (named as E50 and E20), while the II-ECR films were deposited at voltage of −50 V and −20 V (named as I50 and I20) as shown in Fig. 1. The depositing time was 30 min for each sample.

2.2. Carbon film characterization

Raman spectroscopy (HORIBA, LabRAM HR Evolution) was used to study the bonding configuration of carbon films and fitted with a double Gaussian function, the wavelength in Raman spectroscopy was 532 nm C1s and O1s X-ray photoelectron spectra were recorded with a ThermoScientific ESCALAB 250X spectrometer to determine the elemental composition and the quantity of chemical bonds in the carbon film surface. The structures of carbon films were observed by TEM (JEM-3200FS) with electron acceleration voltage of 200 kV. AFM measurements were performed by using a Dimension Edge at room temperature with a BRUKER SCANASYS-AIR tip. The images were recorded in the peak force tapping mode at a scanning rate of 1 Hz with 512 × 512 pixels.

2.3. Electrochemical measurements

Electrochemical experiments were performed by using an electrochemistry workstation of Gamry Reference 600+. A platinum wire and an Ag/AgCl electrode were used as counter and reference electrodes, respectively. The carbon films were used as the working electrodes. The electrochemical impedance spectroscopy (EIS) were measured from 0.1 Hz to 100 kHz with 5 mM $Ru(NH_3)_6^{2+/3+}$ in 1 M KCl, the AC signal was 5 mV. The electrochemical windows were measured by using cyclic voltammetry (CV) in 0.05 M H_2SO_4 with a scanning rate of 100 mV/s. The electrolyte solution was purged with Ar for 30 min to remove the dissolved oxygen, and Ar atmosphere was maintained throughout the experiments. The electrochemical activities were characterized with 1 mM $Ru(NH_3)_6^{2+/3+}$ in 1 M KCl, 1 mM $Fe(CN)_6^{4-/3-}$ in 1 M KCl, 1 mM dopamine in 0.1 M PBS and 1 mM ascorbic acid in 0.1 M phosphate buffer solutions (PBS). The square wave voltammetry of 1 mM 5-mC in 0.1 PBS was tested. The pulse size potential and frequency were 5 mV and 5 Hz, respectively. All electrochemical measurements were repeated at least 3 times with different electrodes at room temperature.

2.4. Chemicals

All the chemicals were analytical grade and used as received. Hexaammineruthenium (III) chloride, dopamine, ascorbic acid and 5-mC were purchased from Shanghai Macklin Biochemical Co., Ltd (China). Potassium ferricyanide was obtained from Sinopharm Chemical Reagent Co., Ltd (China). Potassium chloride was purchased from Xilong Chemical Co., Ltd (China). Sulfuric acid was obtained from Zhuhai huachengda Chemical Co., Ltd (China). PBS were prepared by mixing stock solutions of Na_2HPO_4 and KH_2PO_4. Ultrapure water was used in all experiments.

3. Results and discussion

3.1. Surface structures and chemical composition

The carbon films were characterized with AFM, TEM, Raman spectroscopy and XPS measurements. Firstly, surface roughness (Ra) of carbon films were determined from an area of 5 μm × 5 μm. As shown in Fig. 2, the surface of EI-ECR and II-ECR carbon films were both very flat. The values of Ra were all on the Angstrom (Å) scale as presented in Table 1. They are much lower than GC electrode (typical Ra is 2–4 nm) [3,18]. Meanwhile, comparing with the carbon films prepared by electron beam evaporation, they are almost the same [19]. Furthermore, some obvious protrusions on sample E20 and E50 could be observed in Fig. 2, which maybe related with the formation of graphene nanocrystallite. Thus, EI-ECR carbon films have rougher surfaces than the II-ECR carbon films.

The microstructures of carbon films were characterized with high-resolution TEM as presented in Fig. 3. The samples I50 and I20 prepared by II-ECR were both amorphous structures without any graphene sheets observed. However, graphene nanocrystallite

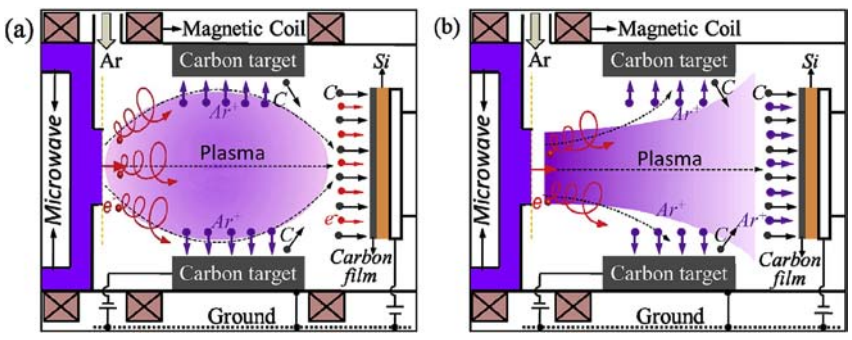

Fig. 1. A schematic illustration of the formation of ER-ECR films (a) and IR-ECR films (b).

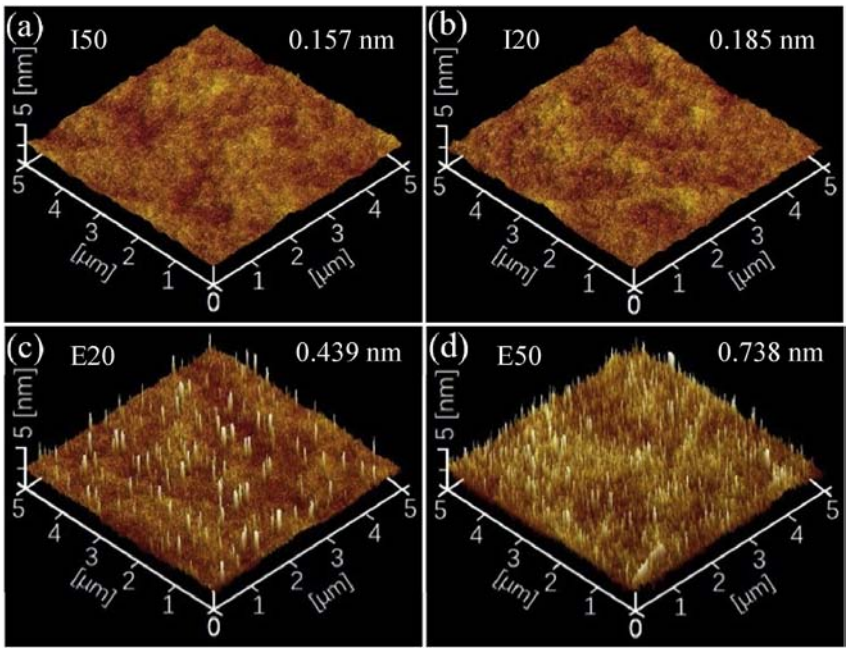

Fig. 2. AFM images of the surface of carbon films: (a) I50; (b) I20; (c) E20; (d) E50.

Table 1
The surface characterization data of carbon films with AFM, Raman and XPS.

	Ra (nm)	I_D/I_G	O/C%	C—O%	C=O%	$sp^2/(sp^2+sp^3)$%
I50	0.157	0.17	7.31	4.51	3.56	62.20
I20	0.185	0.28	6.76	5.19	4.71	71.55
E20	0.439	0.98	5.62	8.48	9.72	85.14
E50	0.738	1.38	5.49	8.31	9.53	86.86

could be found in the samples E20 and E50 prepared by EI-ECR. Each graphene nanocrystallite contained several layers graphene sheets, which showed twisting, curving and vertically oriented to the film surface. The sizes of graphene sheets in sample E50 are larger than that E20. This result indicates that the EI-ECR are favorable to form graphene nanocrystallite structure. It also proved that the higher roughness of EI-ECR carbon films were resulted from the formation of graphene nanocrystallite.

We studied the bonding configuration of carbon films by Raman spectroscopy. As shown in Fig. 4, the Raman spectra of samples I50 and I20 exhibited a strong G peak around 1555 cm^{-1}, which arising from the bond stretching of pairs of sp^2-bonded C atoms in rings and olefinic chains [20]. On the other hand, the Raman spectra of samples E50 and E20 contained separable D and G peak around 1350 cm^{-1} and 1598 cm^{-1}, respectively. The clear-shaped D band represented long range ordered structures with sp^2 hybridization. The G peak shifted to higher frequency compared with II-ECR carbon film, which suggesting the bond ordering or clustering of sp^2 phase towards nanocrystalline carbon [21]. Moreover, the sample E50 exhibited obvious 2D peak, which was arose from the two-phono involved double resonance Raman process and typically occurs inside a graphene layer. It suggests the existence of graphene sheets in samples E50. Furthermore, we obtained the D/G peak ratio I_D/I_G for each spectrum by Breit–Wigner–Fano (BWF) [21,22] fitting as shown in Table 1. I_D/I_G increased from 0.17 to 1.38 with the increasing of bias voltage. I_D/I_G ratio is related to clustering and ordering of the sp^2 phase in stage 2 of Ferrari's model [21]. Since the sp^2 phase clusters, there is a growing number of rings, which increases the D peak intensity and I_D/I_G. The TEM analysis results showed the formation of graphene nanocrystallite in EI-ECR carbon films. Hence, we can conclude that the graphene sheets were formed in EI-ECR carbon films and lead to the increasing of D peak intensity and I_D/I_G in Raman spectroscopy.

Furthermore, the surface chemistry of carbon films was also analyzed by XPS. As showed in Fig. 5, the high-resolution C1s XPS spectra was used to determine the relative concentration of sp^2 and sp^3 hybrid carbons. From the I50 to E50, the shoulder peak observed on the higher energy side of the main large peak decreased with the bias voltage increasing. Based on the Shirley's method [23], the C1s XPS spectra were decomposed into four peaks (C1–C4). The peaks appeared at 284.6 eV (C1, C=C) and 285.5 eV (C2, C–C) are assigned to sp^2 and sp^3 hybrids and colored with red and blue, respectively. The C3 and C4 peaks with purple and green are assigned to C–O and C=O bonds caused by oxygen adsorbed on the carbon film surface. As shown in Table 1, the EI-ECR carbon films contained more C–O and C=O bonds, whereas the ratio of O1s/C1s in EI-ECR carbon films was lower. This indicates that the C–O and C=O bonds are more easy forming at the surface of EI-ECR carbon film. Comparing with II-ECR films, the ratios of $sp^2/(sp^2+sp^3)$ were higher in EI-ECR films. During the low-energy electron irradiation in ECR system, the incident electrons interacted with the carbon atoms on the film top-surface through inelastic scattering, leading the bond transformation from sp^3 to sp^2 and the formation of graphene sheets [15,24]. Moreover, the value of bias voltage denoted the electron irradiation energy. Higher bias voltage lead to more sp^2-bonded carbon. Based on the above results, the TEM image, Raman spectra and XPS are all in good agreement in confirming that EI-ECR carbon films are typical GSEC film with more sp^2-bonded carbons and graphene sheet edges. We can control the film structure gradually from amorphous to graphene sheets embedded structures by IR-ECR and ER-ECR.

3.2. Electrochemical properties

3.2.1. EIS

The EIS were measured to characterize the electrochemical properties of carbon films. The Bode plot and Nyquist plot were

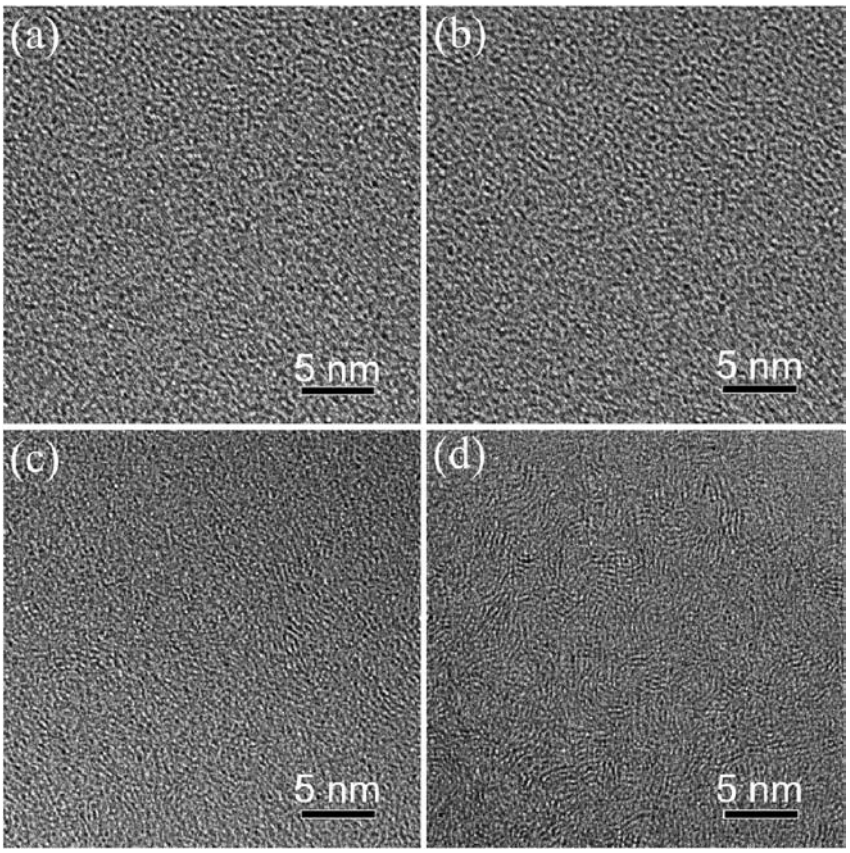

Fig. 3. Surface TEM micrographs of carbon films: (a) I50; (b) I20; (c) E20; (d) E50.

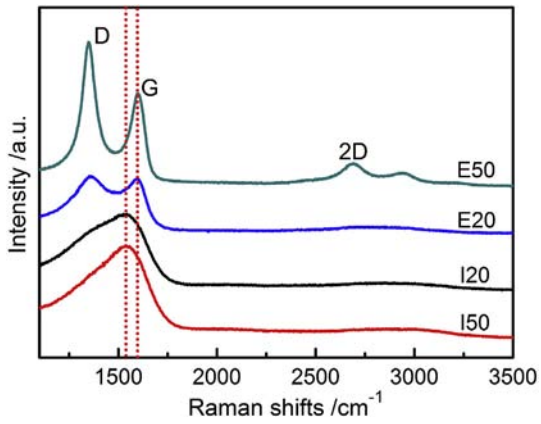

Fig. 4. Raman spectroscopy of four carbon films.

presented in Fig. S1 and Fig. 6(a), respectively. There was only one time-constant observed. At high-frequency range, a very small semi-circle was formed as shown in Fig. 6(b). The straight line in the low-frequency suggested that the response was dominated by diffusion. The EIS data was fitted with the Gamry Echem Analyst software as listed in Table 2. The R_{ct}, R_s, W_d and CPE were the charge transfer resistance, solution resistance, Warburg element and Constant Phase Element, respectively. The parameter n indicated the deviation of CPE's characteristics from an ideal capacitor. When the value of n is 1, it means an ideal capacitor. The double-layer capacitance (C_{dl}) of EI-ECR carbon films were higher than II-ECR carbon films, which may be resulted from the higher surface roughness of EI-ECR carbon films. Based on reference [25], we calculated the apparent heterogeneous rate constant (K^0_{app}). The EI-ECR carbon films had lower R_{ct} and higher K^0_{app}. The $Ru(HN_3)_6^{2+/3+}$ is an outer-sphere redox system, which is not affected by the surface state [1]. The charge transfer resistance can be decomposed into two parts. The one is electron transfer resistance from the redox species in solution to the surface of carbon film, the other is electron transport resistance through the carbon film [25]. Hence, we can conclude that the electron transfer resistance and electron transport resistance in EI-ECR carbon films are lower than II-ECR carbon films.

3.2.2. CV

As an important electrochemical characteristic, the potential windows were measured to confirm the stability of carbon film electrodes for high potential polarization. Based on the report of Granger et al. [26], the potential window was defined as the potential range with the current variation limited in $\pm 500\,\mu A/cm^2$. Fig. 7 showed the CVs of carbon films electrodes in 0.05 M H_2SO_4 with a scanning rate of 100 mV/s we also tested the potential window of GC as reference. The GC electrode surface was polished using 0.05 μm Al_2O_3 particles and ultrasonic cleaned in deionized water before the electrochemical measurements. The potential window of EI-ECR carbon films are a little narrower than II-ECR carbon films, but wider than GC obviously. The values of potential window are mainly influenced by the oxygen evolution reaction overpotential and hydrogen evolution reaction overpotential [27]. The higher the overpotential, the wider the potential window. The kinetics of oxygen and hydrogen evolution reaction are the decisive factor of overpotential value, and strongly depend on the nature of the carbon electrode material as well as the preparation of the

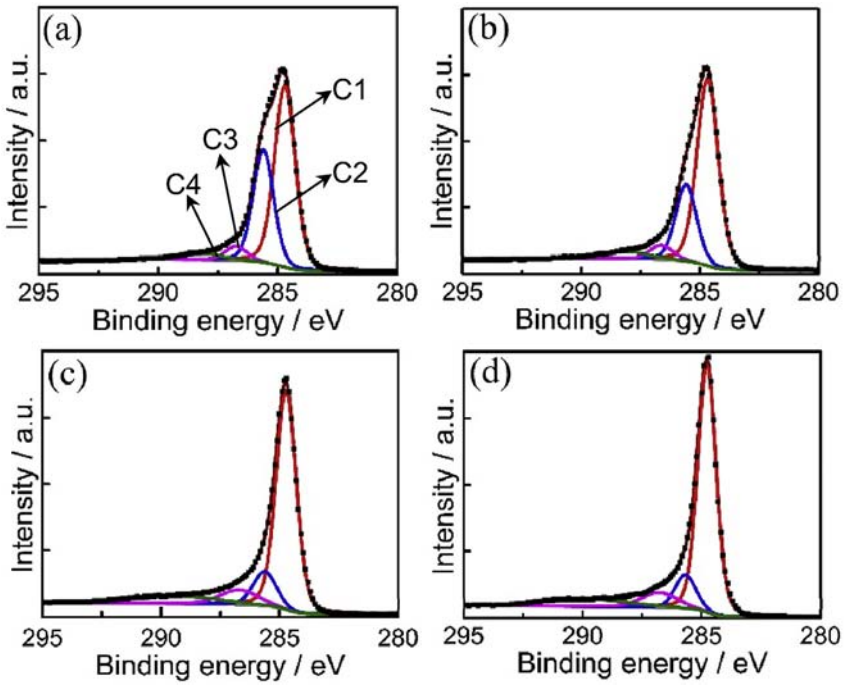

Fig. 5. High-resolution decomposition C 1s XPS spectra of carbon films: (a) I50; (b) I20; (c) E20; (d) E50.

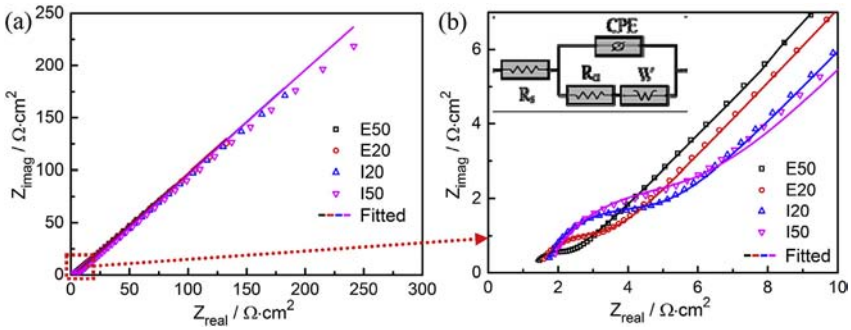

Fig. 6. The full range (a) and high-frequency range (b) Nyquist plots of carbon film electrodes obtained from EIS measurements with 5 mM $Ru(NH_3)_6^{2+/3+}$ in 1 M KCl. The insert is equivalent circuit (The Bode plots showed in Fig. S1).

Table 2
Fitted results of EIS with the equivalent circuit.

Carbon films	$R_s/\Omega\cdot cm^2$	$C_{dl}/\mu F\cdot cm^{-2}$	n	$R_{ct}/\Omega\cdot cm^2$	$W_d \times 10^{-3}/\Omega^{-1}\cdot s^{1/2}$	$K^0_{app}/cm\cdot s^{-1}$
E50	1.39	32.18	0.834	1.195	10.29	0.090
E20	1.63	24.31	0.868	1.804	6.87	0.060
I20	1.45	15.26	0.890	3.004	5.01	0.036
I50	1.62	14.06	0.883	4.131	3.76	0.026

surface [1]. For the carbon materials, the relative concentration of sp^2 and sp^3 hybrid carbons have great influence on the density of electronic states (DOS). DOS of the carbon film can increase electron transfer rate and reduce the overpotential, such as the relationship between sp^2-bond content and the potential window reported by Jia et al. [28]. The DOS of sp^2 carbon atoms were higher than sp^3 carbon atoms in the vicinity of the Fermi level [29,30], and the graphene edge sites were easier to gain more electron by calculating the profiles of Mulliken charge [31,32]. Hence, we can conclude that the DOS of EI-ECR carbon films was higher than II-ECR carbon films by comparing the relative concentration of sp^2 and sp^3 hybrid carbons and the amount of graphene edges. Therefore, the potential windows of GSEC films were lower than amorphous carbon films. Besides the influence of carbon structure, higher surface roughness and oxygen-containing groups contents could also reduce the potential window [3]. As shown in Fig. 2 and Table 1, EI-ECR carbon films possessed higher roughness and more oxygen-containing groups, which also caused the GSEC film showed a narrow potential window than II-ECR films.

In order to examine the electrochemical activity of these carbon films, several redox systems were used in CVs measurements including $Ru(NH_3)_6^{2+/3+}$, $Fe(CN)_6^{4-/3-}$, DA and AA. Fig. 8(a)

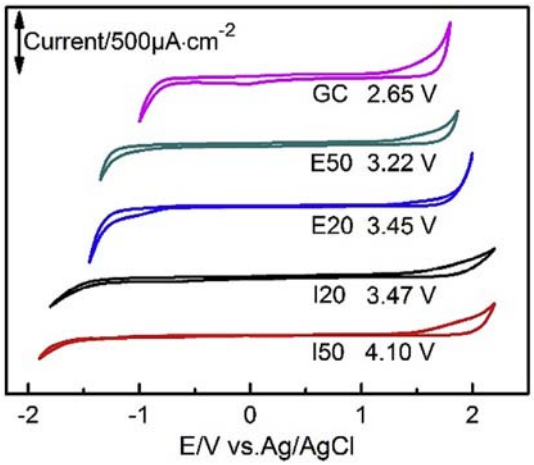

Fig. 7. Voltammograms of ECR carbon films electrodes in 0.05 M H_2SO_4 deoxygenated with Ar (Scan rate, 100 mV/s).

presented the CVs of 1 mM $Ru(NH_3)_6^{2+/3+}$ in 1 M KCl at four carbon film electrodes with a scanning rate of 100 mV/s. The oxidation-reduction peak separation (ΔE_P) of $Ru(NH_3)_6^{2+/3+}$ were calculated as showed in Table 3. The ΔE_P of $Ru(NH_3)_6^{2+/3+}$ at EI-ECR carbon film electrodes were lower than II-ECR carbon film electrodes. The higher the bias voltage, the lower ΔE_P. It is well-established that $Ru(NH_3)_6^{2+/3+}$ is considered to be a simple outer-sphere redox system, which means the electron-transfer rate is insensitive to surface chemistry, including the surface functional groups, surface roughness, the monolayer adsorption [1]. The most important factor affecting the reaction rate of $Ru(NH_3)_6^{3+/2+}$ is the electronic structure of electrode [33]. The EI-ECR carbon films had higher DOS due to the more content of sp^2 carbons and nanosized graphene sheets as former discussed. The EIS results further showed the electron transfer resistance and electron transport resistance of EI-ECR carbon films were lower than II-ECR carbon films. It means that the electron can be more easily transferred and transported in graphene sheets. Therefore, the ΔE_P of $Ru(NH_3)_6^{2+/3+}$ at EI-ECR carbon film is lower than II-ECR carbon film, and the EI-ECR carbon film has better electrochemical activity in $Ru(NH_3)_6^{2+/3+}$ solution.

The CVs of 1 mM $Fe(CN)_6^{3-/4-}$ at four carbon film electrodes were presented in Fig. 8(b). It showed the peak current of EI-ECR carbon films were higher than II-ECR carbon films, which may be related with the higher active surface area. The values of active surface area of samples E50, E20, I20 and I50 were evaluated with the Randles-Sevcik equation [34], and they were 1.039 cm^2, 0.944 cm^2, 0.873 cm^2 and 0.827 cm^2 (the CVs were showed in Fig. S2), respectively. The ΔE_P at a scanning rate of 100 mV/s were listed in Table 3. The ΔE_P of $Fe(CN)_6^{3-/4-}$ at EI-ECR carbon films were much lower than that at II-ECR carbon films, and the ΔE_P at sample E50 was lower than sample E20. It suggested that the EI-ER carbon films had better electrochemical activity than II-ECR carbon films in $Fe(CN)_6^{3-/4-}$. As an inner-sphere redox couple, the kinetics of $Fe(CN)_6^{3-/4-}$ is dependent on the surface chemistry, electronic properties and surface cleanliness [35,36]. The influence of surface cleanliness can be ignored due to the same treatments for all the

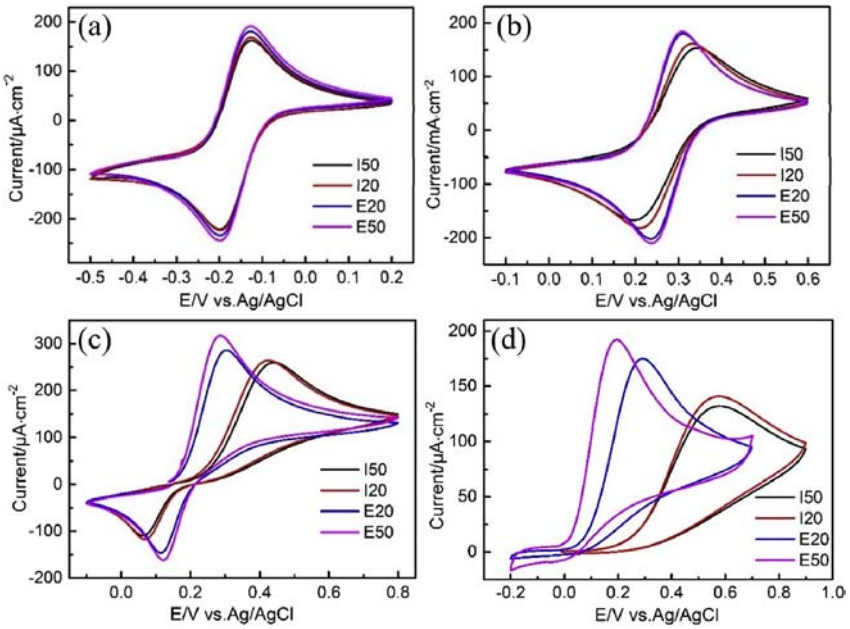

Fig. 8. CVs of carbon film electrodes with (a) 1 mM $Ru(NH_3)_6^{2+/3+}$ in 1 M KCl, (b) 1 mM $Fe(CN)_6^{4-/3-}$ in 1 M KCl, (c) 1 mM DA in 0.1 M PBS and (d) 1 mM AA in 0.1 M PBS, scan rate, 100 mV/s.

Table 3
The value of potential window and △Ep in several redox system.

	Potential window/V	△Ep $Ru(NH_3)_6^{2+/3+}$/mV	△Ep $Fe(CN)_6^{4-/3-}$/mV	△Ep DA/mV	Oxidation Potential AA/mV
I50	4.10	75.8	145.8	377.1	576.5
I20	3.47	73.8	121.7	359.1	574.8
E20	3.45	71.9	73.9	189.9	288.9
E50	3.22	69.9	71.3	164.2	194.2

samples during the experiments. As reported by McCreery [36,37] and several other groups [38,39], the electron-transfer rate of $Fe(CN)_6^{3-/4-}$ at carbon electrodes was dependent on the amount of exposed graphene edges sp^2 carbon instead of the amount of surface oxygen. The effect of surface oxygen can be neglected. The film structure was the major factor to influence the electrochemical activity. As shown in Fig. 9(a), the GSEC films have lots of nanosized graphene sheets. The edges in GSEC film can offer more reactive sites for $Fe(CN)_6^{3-/4-}$ redox as shown in the left of Fig. 9(b). More reactive sites are helpful to reduce the electron transfer resistance. Therefore, the electron can be more easily transferred between graphene sheets edge carbon atoms and solution, which resulted in the lower ΔE_P of $Fe(CN)_6^{3-/4-}$ on EI-ECR films than II-ECR films. Hence, it is the graphene edges induced the higher electrochemical activity of GSEC films than amorphous carbon films in $Fe(CN)_6^{3-/4-}$ redox system.

The CVs of 1 mM DA and 1 mM AA in 0.1 M PBS at four carbon film electrodes were shown at Fig. 8(c) and (d), respectively. It suggested that the oxidation peak current density of DA and AA on EI-ECR films were both higher than II-ECR films. The higher oxidation peak current density maybe related with the higher active surface area. Since the oxidation of AA was totally irreversible and no reduction peak was observed on the cyclic voltammograms, the oxidation peak potential values were compared instead of ΔE_P as shown in Table 3. Comparing with II-ECR carbon films, the ΔE_P of DA and AA at EI-ECR carbon films are much lower. The ΔE_P of DA on EI-ECR carbon films are also much lower than the carbon films prepared by Jia J [28] with II-ECR. It suggested that the EI-ECR carbon films had better electrochemical activity than II-ECR carbon films in DA and AA solutions. The DA and AA are both catechol derivatives, which electrochemical oxidation reaction process is diffusion controlled [40]. The catechol derivatives are surface sensitive redox system and require adsorption to the surface to undergo oxidation [41]. The sp^2-bonded graphene sheets edges of EI-ECR carbon film is helpful to form π-π interaction between the surface sp^2 bonds and polar aromatic [36], which induce the GSEC film possesses better adsorption ability for catechol derivatives. The surface oxygen functional groups have no influence on DA [41], and

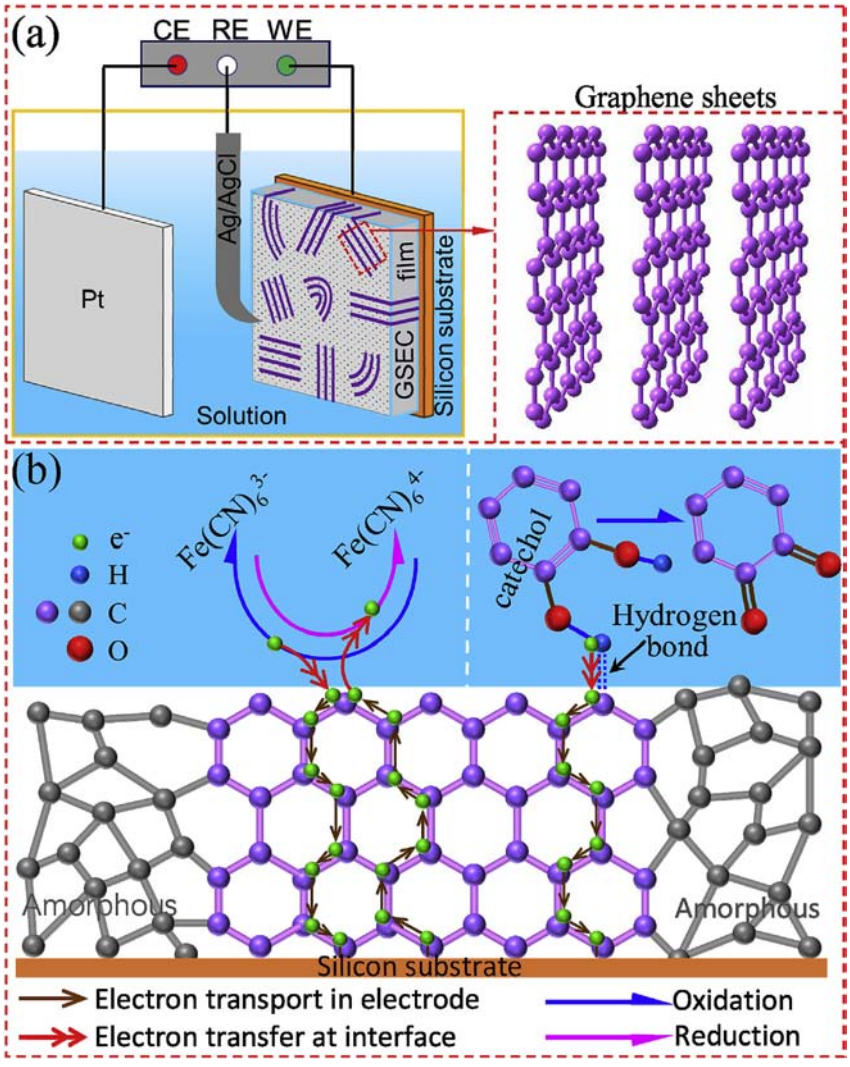

Fig. 9. (a) The schematic diagram of three-electrode cell. The counter electrode (CE), reference electrode (RE) and working electrode (WE) are Pt, Ag/AgCl, and GSEC film, respectively. The insert is graphene sheets formed in carbon film. (b) The high electrochemical activity of GSEC film originated from the graphene sheets: (i) graphene sheets edges as active sites are beneficial to increase the electron transfer rate between the electrode and solution as denoted by the red double arrows; (ii) the graphene sheets offer fast electron transport paths in GSEC film as denoted by the brown arrows. In $Fe(CN)_6^{3-/4-}$ solution, the edge carbon atoms as active sites reduced electron transfer resistance and increased the electron transfer rate. In catechol derivations solutions, the graphene sheets edges as hydrogen bonding sites facilitate proton-assisted electron transfer and the oxidation of catechol derivations, resulted in the high electrochemical activity of GSEC film.

the electrostatic repulsion between DA and surface oxygen functional groups can be neglected in neutral pH solution, because the amine group in DA is protonated giving it a positive charge [36]. Based on the "self-catalysis" mechanism [42], the graphene sheets edges can be taken as hydrogen bonding sites, and facilitate the proton-assisted electron transfer as shown in Fig. 9(b). Therefore, the oxidation potential of DA at EI-ECR carbon film is lower than that at II-ECR carbon film, and we can conclude that the GSEC films have electrocatalytic property for the oxidation of DA.

For the AA, its sensitivity to oxygen functional groups is debated. Chen P et al. [36] classified AA as a surface sensitive but not oxide sensitive redox system, however, some other researchers showed that the amorphous carbon films with lower oxygen content [20] and vacuum heat-treated GC [43] had higher reactivity toward the oxidation of AA. It has been proposed that the AA is negatively charged at neutral pH and may be affected by electrostatic repulsion of surface oxygen functional groups. The XPS showed the EI-ECR carbon films had more C—O and C═O bonds, but the EI-ECR carbon films showed better reactivity than II-ECR carbon films. Therefore, we inferred the key factor was the nanosized graphene sheets in carbon film instead of surface oxygen functional groups. The nanosized graphene sheets offer more active sites, which helpful to the formation of hydrogen bonds between the AA and graphene sheets [10]. Hence, the GSEC films exhibit better electrochemical activity for the oxidation of AA than II-ECR carbon films.

3.3. Application of detecting biomolecules

The wide potential window and high electrochemical activity of EI-ECR carbon films means it can be used to detect biomolecules with high oxidation potential. 5-Methylcytosine (5-mC) is an important DNA base because it contains heritable information and often associates with transcriptional silence of tumor suppressor genes [44]. The 5-mC is often regarded as a hallmark of various human cancers [45]. The detection of 5-mC is very important to understand the molecular pathology for early cancer diagnosis. However, the classical GC electrodes can not be used since the high oxidation potential of 5-mC. The Fig. 10 showed the square wave voltammetrys of 1 mM 5-mC in 0.1 PBS at ECR carbon film electrodes. The oxidation potential of 5-mC at I50, I20, E20 and E50 were 1.48 V, 1.45 V, 1.32 V and 1.27 V, respectively. The 5-mC oxidized at lower potential on EI-ECR carbon film surface than that on II-ECR carbon film. This further proved that the improved electrocatalytic property of EI-ECR carbon film. Meanwhile, the detecting current density of EI-ECR carbon films are larger than that of II-ECR carbon films, especially the sample E50. The signal-to-noise of E50, E20, I20 and I50 were 8.85, 4.13, 6.35 and 5.5, respectively. It indicats that the EI-ECR carbon films possesses good electrochemical activity in detecting 5-mC. All these results indicate the GSEC film is a potential electrochemical biosensor material in detecting biomolecules with high oxidation potential.

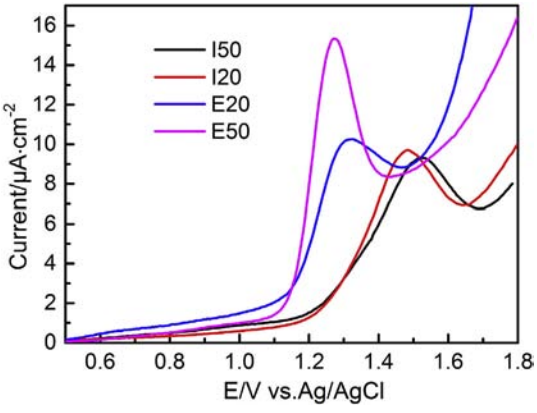

Fig. 10. Square Wave Voltammetrys of 1 mM 5-mC in 0.1 PBS at ECR carbon film electrodes.

4. Conclusion

The electrochemical performances of graphene sheets embedded carbon (GSEC) films were investigated by electrochemical impedance spectroscopy and cyclic voltammetry. The GSEC films showed lower charge-transfer resistance in $Fe(CN)_6^{3-/4-}$ solution, and lower ΔE_P in both outer-sphere and inner-sphere redox system than amorphous carbon films. GSEC films exhibited high electrochemical activity while maintained a wide potential window over 3.2 V. This GSEC film also showed reactivity and electrocatalytic property in the application of detecting 5-Methylcytosine. The mechanisms are the nanosized graphene sheets increased electron-transport rate and the graphene edges offered more reaction active sites. Our GSEC films showed great potential to be an electrochemical biosensor in detecting biomolecules with high oxidation potential.

Acknowledgements

The authors would like to acknowledge the National Nature Science Foundation of China (Grant Numbers 51575359 and 11404217) and Shenzhen Fundamental Research subject-layout project (Grant Number JCYJ20160427105015701).

Appendix A. Supplementary data

Supplementary data related to this article can be found at https://doi.org/10.1016/j.electacta.2018.01.027.

References

[1] R.L. McCreery, Advanced carbon electrode materials for molecular electrochemistry, Chem. Rev. 108 (2008) 2646–2687.
[2] R.G. Compton, J.S. Foord, F. Marken, Electroanalysis at diamond-like and doped-diamond electrodes, Electroanalysis 15 (2003) 1349–1363.
[3] N. Sekioka, D. Kato, A. Ueda, T. Kamata, R. Kurita, S. Umemura, S. Hirono, O. Niwa, Controllable electrode activities of nano-carbon films while maintaining surface flatness by electrochemical pretreatment, Carbon 46 (2008) 1918–1926.
[4] T.Y. You, O. Niwa, M. Tomita, T. Ichino, S. Hirono, Electrochemical oxidation of alkylphenols on ECR-sputtered carbon film electrodes with flat sub-nanometer surfaces, J. Electrochem. Soc. 149 (2002) E479–E484.
[5] T. Kamata, D. Kato, H. Ida, O. Niwa, Structure and electrochemical characterization of carbon films formed by unbalanced magnetron (UBM) sputtering method, Diam. Relat. Mater. 49 (2014) 25–32.
[6] H. Yanagisawa, R. Kurita, T. Yoshida, T. Kamata, O. Niwa, Electrochemical assessment of local cytosine methylation in genomic DNA on a nanocarbon film electrode fabricated by unbalanced magnetron sputtering, Sensor. Actuator. B Chem. 221 (2015) 816–822.
[7] W. Zhang, S. Zhu, R. Luque, S. Han, L. Hu, G. Xu, Recent development of carbon electrode materials and their bioanalytical and environmental applications, Chem. Soc. Rev. 45 (2016) 715–752.
[8] Y. Shao, J. Wang, H. Wu, J. Liu, I.A. Aksay, Y. Lin, Graphene based electrochemical sensors and biosensors: a review, Electroanalysis 22 (2010) 1027–1036.
[9] G. Yildiz, Z. Aydogmus, M.E. Cinar, F. Senkal, T. Ozturk, Electrochemical oxidation mechanism of eugenol on graphene modified carbon paste electrode and its analytical application to pharmaceutical analysis, Talanta 173 (2017) 1–8.
[10] Z.-H. Sheng, X.-Q. Zheng, J.-Y. Xu, W.-J. Bao, F.-B. Wang, X.-H. Xia, Electrochemical sensor based on nitrogen doped graphene: simultaneous determination of ascorbic acid, dopamine and uric acid, Biosens. Bioelectron. 34 (2012) 125–131.
[11] V.V. Sharma, I. Gualandi, Y. Vlamidis, D. Tonelli, Electrochemical behavior of reduced graphene oxide and multi-walled carbon nanotubes composites for catechol and dopamine oxidation, Electrochim. Acta 246 (2017) 415–423.

[12] S. Shiba, J. Inoue, D. Kato, K. Yoshioka, O. Niwa, Graphene modified electrode for the direct electron transfer of bilirubin oxidase, Electrochemistry 83 (2015) 332–334.
[13] C. Wang, X. Zhang, D.F. Diao, Nanosized graphene crystallite induced strong magnetism in pure carbon films, Nanoscale 7 (2015) 4475–4481.
[14] L. Yang, G.J. Hu, D.Q. Zhang, D.F. Diao, Nanosized graphene sheets enhanced photoelectric behavior of carbon film on p-silicon substrate, Appl. Phys. Lett. 109 (2016), 031910.
[15] C. Wang, D.F. Diao, X. Fan, C. Chen, Graphene sheets embedded carbon film prepared by electron irradiation in electron cyclotron resonance plasma, Appl. Phys. Lett. 100 (2012), 231909.
[16] C. Chen, D.F. Diao, X. Fan, L. Yang, C. Wang, Frictional behavior of carbon film embedded with controlling-sized graphene nanocrystallites, Tribol. Lett. 55 (2014) 429–435.
[17] C. Wang, D.F. Diao, Magnetic behavior of graphene sheets embedded carbon film originated from graphene nanocrystallite, Appl. Phys. Lett. 102 (2013), 052402.
[18] A. Ueda, D. Kato, N. Sekioka, T. Kamata, R. Kurita, H. Uetsuka, Y. Hattori, S. Hirono, S. Umemura, O. Niwa, Fabrication of electrochemically stable fluorinated nano-carbon film compared with other fluorinated carbon materials, Carbon 47 (2009) 1943–1952.
[19] N. Yang, H. Uetsuka, H. Watanabe, T. Nakamura, C.E. Nebel, Photochemical amine layer formation on H-Terminated single-crystalline CVD diamond, Chem. Mater. 19 (2007) 2852–2859.
[20] T. Palomäki, N. Wester, L.-S. Johansson, M. Laitinen, H. Jiang, K. Arstila, T. Sajavaara, J.G. Han, J. Koskinen, T. Laurila, Characterization and electrochemical properties of oxygenated amorphous carbon (a-C) films, Electrochim. Acta 220 (2016) 137–145.
[21] A.C. Ferrari, J. Robertson, Interpretation of Raman spectra of disordered and amorphous carbon, Phys. Rev. B 61 (2000) 14095–14107.
[22] D.G. McCulloch, S. Prawer, A. Hoffman, Structural investigation of xenon-ion-beam-irradiated glassy carbon, Phys. Rev. B 50 (1994) 5905–5917.
[23] J. Díaz, G. Paolicelli, S. Ferrer, F. Comin, Separation of the sp^3 and sp^2 components in the C1s photoemission spectra of amorphous carbon films, Phys. Rev. B Condens. Matter 54 (1996) 8064–8069.
[24] C. Chen, X. Fan, D. Diao, Low-energy electron irradiation induced top-surface nanocrystallization of amorphous carbon film, Appl. Surf. Sci. 384 (2016) 341–347.
[25] T. Palomäki, N. Wester, M.A. Caro, S. Sainio, V. Protopopova, J. Koskinen, T. Laurila, Electron transport determines the electrochemical properties of tetrahedral amorphous carbon (ta-C) thin films, Electrochim. Acta 225 (2017) 1–10.
[26] M.C. Granger, J.S. Xu, J.W. Strojek, G.M. Swain, Polycrystalline diamond electrodes: basic properties and applications as amperometric detectors in flow injection analysis and liquid chromatography, Anal. Chim. Acta 397 (1999) 145–161.
[27] H.B. Martin, A. Argoitia, U. Landau, A.B. Anderson, J.C. Angus, Hydrogen and oxygen evolution on boron-doped diamond electrodes, J. Electrochem. Soc. 143 (1996) L133–L136.
[28] J.B. Jia, D. Kato, R. Kurita, Y. Sato, K. Maruyama, K. Suzuki, S. Hirono, T. Ando, O. Niwa, Structure and electrochemical properties of carbon films prepared by a electron cyclotron resonance sputtering method, Anal. Chem. 79 (2007) 98–105.
[29] X. Jiang, J. Zhao, Y.-L. Li, R. Ahuja, Tunable assembly of sp^3 cross-linked 3D graphene monoliths: a first-principles prediction, Adv. Funct. Mater. 23 (2013) 5846–5853.
[30] H. Bu, M. Zhao, A. Wang, X. Wang, First-principles prediction of the transition from graphdiyne to a superlattice of carbon nanotubes and graphene nanoribbons, Carbon 65 (2013) 341–348.
[31] X. Zhang, C. Wang, C.Q. Sun, D.F. Diao, Magnetism induced by excess electrons trapped at diamagnetic edge-quantum well in multi-layer graphene, Appl. Phys. Lett. 105 (2014), 042402.
[32] A.S. Barnard, I.K. Snook, Size- and shape-dependence of the graphene to graphane transformation in the absence of hydrogen, J. Mater. Chem. 20 (2010) 10459–10464.
[33] P. Chen, M.A. Fryling, R.L. McCreery, Electron transfer kinetics at modified carbon electrode surfaces: the role of specific surface sites, Anal. Chem. 67 (1995) 3115–3122.
[34] A.J. Bard, L.R. Faulkner, Electrochemical Methods: Fundamental and Applications, second ed., John Wiley and Sons, New York, 2001.
[35] Y. Tanaka, M. Furuta, K. Kuriyama, R. Kuwabara, Y. Katsuki, T. Kondo, A. Fujishima, K. Honda, Electrochemical properties of N-doped hydrogenated amorphous carbon films fabricated by plasma-enhanced chemical vapor deposition methods, Electrochim. Acta 56 (2011) 1172–1181.
[36] P.H. Chen, R.L. McCreery, Control of electron transfer kinetics at glassy carbon electrodes by specific surface modification, Anal. Chem. 68 (1996) 3958–3965.
[37] R.J. Bowling, R.T. Packard, R.L. McCreery, Activation of highly ordered pyrolytic graphite for heterogeneous electron transfer: relationship between electrochemical performance and carbon microstructure, J. Am. Chem. Soc. 111 (1989) 1217–1223.
[38] H. Kaneko, A. Negishi, Y. Suda, T. Kawakubo, Fabrication and evaluation of pfc (plastic formed carbon) electrodes for voltammetric use, Denki Kagaku 61 (1993) 920–921.
[39] C.E. Banks, R.G. Compton, New electrodes for old: from carbon nanotubes to edge plane pyrolytic graphite, Analyst 131 (2006) 15–21.
[40] F. Wantz, C.E. Banks, R.G. Compton, Direct oxidation of ascorbic acid at an edge plane pyrolytic graphite electrode: a comparison of the electroanalytical response with other carbon electrodes, Electroanalysis 17 (2005) 1529–1533.
[41] S.H. DuVall, R.L. McCreery, Control of catechol and hydroquinone electron-transfer kinetics on native and modified glassy carbon electrodes, Anal. Chem. 71 (1999) 4594–4602.
[42] S.H. DuVall, R.L. McCreery, Self-catalysis by catechols and quinones during heterogeneous electron transfer at carbon electrodes, J. Am. Chem. Soc. 122 (2000) 6759–6764.
[43] D.T. Fagan, I.F. Hu, T. Kuwana, Vacuum heat-treatment for activation of glassy carbon electrodes, Anal. Chem. 57 (1985) 2759–2763.
[44] T. Ushijima, Innovation - detection and interpretation of altered methylation patterns in cancer cells, Nat. Rev. Canc. 5 (2005) 223–231.
[45] D. Kato, N. Sekioka, A. Ueda, R. Kurita, S. Hirono, K. Suzuki, O. Niwa, A nanocarbon film electrode as a platform for exploring DNA methylation, J. Am. Chem. Soc. 130 (2008) 3716–3717.